Journal Pre-proof

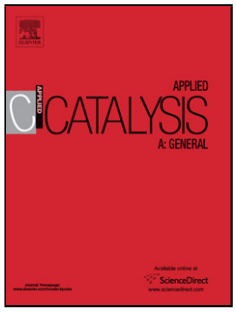

Furfural hydrodeoxygenation on iron and platinum catalysts

Zanuttini M. Soledad, Gross Martin, Marchetti Gustavo, Querini, Carlos

PII: S0926-860X(19)30372-2

DOI: https://doi.org/10.1016/j.apcata.2019.117217

Article Number: 117217

Reference: APCATA 117217

To appear in: *Applied Catalysis A: General*

Received Date: 12 April 2019

Revised Date: 19 July 2019

Accepted Date: 24 August 2019

Please cite this article as: Zanuttini MS, Gross M, Marchetti G, Querini, C, Furfural hydrodeoxygenation on iron and platinum catalysts, *Applied Catalysis A, General* (2019), doi: https://doi.org/10.1016/j.apcata.2019.117217

Furfural hydrodeoxygenation on iron and platinum catalysts

Zanuttini, M. Soledad[1]*; Gross, Martin[1]; Marchetti[2], Gustavo; Querini, Carlos[1].

[1] *Instituto de Investigaciones en Catálisis y Petroquímica "Ing. José Miguel Parera" (INCAPE) – CONICET - Universidad Nacional del Litoral, Predio CONICET Dr. Alberto Cassano, Colectora Ruta Nac. N 168 km. 0, Pje El Pozo, 3000, Santa Fe, Argentina.*

[2] *Centro de Investigación y Desarrollo en Ciencias Aplicadas "Dr Jorge J. Ronco"- CINDECA (UNLP-CONICET). Calle 47 N° 257, (1900) La Plata, Bs. As. Argentina*

CorrespondingAuthor:

Carlos Alberto Querini

E-mail: querini@fiq.unl.edu.ar

Postal Address: Predio CCT Santa Fe- Paraje El Pozo - Colectora Ruta Nac. 168, km 0 – (3000) Santa Fe – Argentina

Tel: +54-342-4533858

Fax: +54-342-4531068

Graphical abstract

GRAPHICAL ABSTRACT

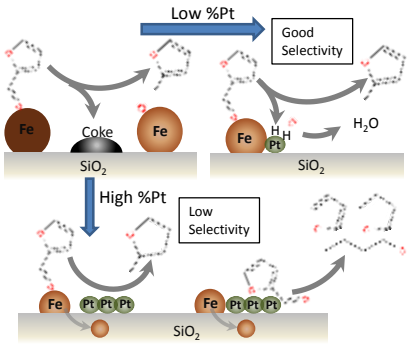

Highlights

- Monometallic iron catalyst shows more than 90% selectivity to 2-methylfuran but poor stability.
- Adding platinum to an iron catalyst affects furfural hydrodeoxygenation conversion, product distribution and stability.
- Low loading of Pt is enough to improve the Fe stability maintaining a good selectivity to 2-MF.
- Fe-Pt catalyst supported on silica can be regenerated.
- Fe and Pt form an alloy.

Abstract

Furfural can be converted into a wide range of high-octane products like 2-methylfuran (2-MF) through hydrodeoxygenation (HDO). Iron-based catalyst (Fe/SiO_2), has shown high selectivity for gas phase conversion of furfural to 2-MF at atmospheric pressure and 573 K. However, it showed rapid deactivation. Furfural is the main coke precursor, although coke is also formed when 2-MF and furan are used as reactants, but in lower quantities. Coke profiles along the catalytic bed suggest that tetra-hydrofuran is an important coke precursor. The addition of a second metal like platinum, even in very low proportions, generates hydrogen spillover leading to an important improvement in the stability of the catalyst. The Fe/Pt ratio on the surface regulates the amount of coke

deposited because it modifies the iron particle sizes, the interaction with the support and the amount of hydrogen available for the reactions. These phenomena influence the reaction, coke formation and regeneration mechanisms.

Keywords: furfural hydrodeoxygenation; iron; platinum; silica

1. INTRODUCTION

Biofuels are important not only because they represent a new way of obtaining energy with CO_2 saving, but also because they can be locally generated, securing fuel supply [1]. Due to its abundance and the variety of products that can be obtained from lignocellulosic biomass, it is a very attractive resource. In this sense, furfural is a potential platform for biofuels and fine chemicals. It can be obtained as a by-product during the conversion of C_5 sugars to ethanol and also, as an important fraction of the fast pyrolysis oil obtained from biomass. This molecule can be converted into a wide range of high-octane products that can be used as gasoline octane boosters [2]. The most promising one is 2-methylfuran (2-MF), being the catalytic hydrodeoxygenation (HDO) the better alternative to obtain this compound [3, 4].

The furfural HDO reaction can be performed at atmospheric pressure at low H_2 partial pressure, being possible to obtain high selectivities depending on the catalyst used. Neither complete hydrogenation nor decarboxylation is desirable. Platinum, palladium and nickel catalysts show high stabilities and also high selectivity to furan (F), and produce ring opening and over-hydrogenated compounds as byproducts. These products are undesirable molecules in this process. DFT studies suggested that furfural adsorbs on Pd through both C=C and C=O bonds whereas on Pt it adsorbs only through the C=C bond present in the ring. However, furfural adsorption is stronger on Pd(111) than on Pt(111) [5]. This is the cause of a faster ring opening on Pd than on Pt at 385 K. Nickel behaves similarly to Pd, tending to adsorb carbonyl group parallel to the surface and, as a consequence, high selectivities to furan and ring-opening products are obtained.

On the other hand, copper or iron-based catalysts have shown high selectivity for the conversion of furfural to furfuryl alcohol or 2-MF but also, they were rapidly deactivated [1]. By DFT and IR spectroscopy studies it was found that on Cu or Fe catalysts, furfural

molecules preferably adsorbs on the metal through the O of the carbonyl group [6]. Similarly, S. Xu et al. [7] concluded that in the case of Pd-Fe catalysts supported on carbon nanotubes, the Fe promotes the formation of Pd nanoparticles and modifies the *d*-band center decreasing the adsorption energy of C=O of glucose and OH of hexitol. DFT studies on Mo_2C also indicated that there is a strong interaction between C=O bond of furfural and the catalyst surface, leading to high selective conversion to 2-mehtylfuran (60% at 425 K). However, heavy compounds (C_{10}) were the second major product, with 30% of selectivity [8].

Based on these observations, several bimetallic catalysts such as Ni-Fe, Pd-Cu, Pd-Fe and Pt-Co have been recently studied. Pd-Cu catalyst greatly suppressed furan production but only furfuryl alcohol was obtained [9]. Wang et al. [4] reported that nanocrystals of $PtCo_3$/C (10% load) catalysts showed high stability and selectivity to 2-MF at low H_2 pressure. Selective conversion of furfural to methylfuran on Ni-Fe bimetallic catalysts was also studied by Sitthisa et al. [3] and Wang et al. [4]. They concluded that the addition of iron to nickel catalyst (Ni(5.0)Fe(2.0)), resulted in a clear enhancement of the yield to 2-methylfuran. The authors reported 40% of selectivity to this product. Pino et al. [10] suggested that the properties of the support have significant influence on the catalytic performance of the bimetallic Pd-Fe catalysts. A selectivity to methylfuran of approximately 60% was obtained with Pd(1.0)Fe(0.5)/SiO_2.

The hydrogenation of furfural into furfuryl alcohol over magnetic γ-Fe_2O_3 was studied using alcohols as hydrogen donors [11]. In this case, instead of using a metal like Pt or Pd to activate the hydrogen, an alcohol is use in order to provide this compound.

Due to its high selectivity to 2-MF and its ability to form bimetallic alloys with Pd, Ni, and Pt, the iron has attracted significant interest. The aim of this work is to study the activities and selectivities obtained with an iron-based catalyst promoted with platinum in the furfural hydrodeoxygenation reaction. Particularly, the platinum-iron synergy and how their proportion affects furfural conversion and the selectivity to 2-methylfuran are addressed. The influence of Fe-Pt ratio supported on silica in product distribution and stability, as well as the catalyst deactivation and regeneration are included in this work.

2. EXPERIMENTAL

2.1 Catalyst preparation

Platinum-iron catalysts supported on silica *(Alfa Aesar large pore)* were prepared by wet impregnation. Tetraammineplatinum (II) nitrate (metal content 50%) supplied by *Alfa Aesar* and iron nitrate nona-hydrated *(Biopack)* were used as precursors. The monometallic catalysts were prepared from a suspension of silica in the metal precursor solution prepared in deionized water *(Sintorgan)*, stirring on a hot plate at 383 K until complete evaporation. The impregnated catalyst was dried in stove at 383 K for 12 h. The dried solid was calcined in air stream in an electric furnace at 623 K (platinum catalyst) or 773 K (iron catalysts), for 2 h. The metallic contents used in this work were selected from previous studies carried out using other model molecules of bio-oil, such as phenol, m-cresol and anisole. The monometallic catalysts are Pt(1.7)/SiO_2 ($Pt_{1.7}$), and Fe(15.0)/SiO_2 (Fe_{15}) [12-14]. Besides, a Fe(5.0)/SiO_2 catalyst (Fe_5), and an iron-free silica sample were prepared repeating the same procedure, for comparison purposes.

Bimetallic catalysts with different Pt-Fe ratio were prepared by co-impregnation: Fe(5.0)Pt(0.5)/SiO_2, ratio Fe/Pt = 10 ($Fe_5Pt_{0.5}$); Fe(7.0)Pt(0.07)/SiO_2, ratio Fe/Pt = 100 ($Fe_7Pt_{0.07}$). A suspension of silica in solution of both platinum and iron precursors was stirred on a hot plate at 383 K until complete evaporation. Then, the solid was dried at 383 K for 12 h and calcined at 773 K for 2 h.

The quantification of the actual values of the metal charges in the catalysts where obtained by Energy Dispersive X-ray Fluorescence Spectroscopy using a Shimadzu EDX-720 spectrometer.

The calcined catalysts were reduced in situ with pure H_2 (30 $ml.min^{-1}$) for 1 h before furfural HDO. Metal-free silica sample was also pretreated with H_2 stream at 773 K for 1 h before characterization analyses and reaction tests.

2.2 Catalysts Characterization

BET surface areas were obtained by nitrogen adsorption technique using a Micrometrics ASAP 2020 analyzer. Pore volumes were estimated by means of the t-plot method.

The X-ray diffractograms of the catalyst were obtained with a Shimadzu XD-D1 instrument with monochromator using CuKα radiation (30 kV, 40 mA) at a scanning rate of 4 $^{o}\cdot min^{-1}$, 2θ = 5º-100º. The crystallite size of α-Fe was determined by the Scherrer's formula based on the main iron peak at 44.71°.

Reducibility of metallic catalysts was studied by temperature programmed reduction experiments (TPR) with an OKHURATP-2002S system, equipped with a thermal conductivity detector (TCD). TPR runs were carried out with a heating rate of 10 $K \cdot min^{-1}$ in 5% H_2/Ar (30 $ml \cdot min^{-1}$). The temperature was increased from 293 to 1173 K.

The acidity of the support was studied by two techniques: Pyridine-Temperature-Programmed Desorption (Py-TPD) and FTIR analyses of pyridine adsorbed on the samples (Py-IR). For Py-TPD technique, the sample was pretreated *in situ* in N_2 flow at 625 K for 1 h. After cooling down to room temperature, the sample was saturated with pyridine. Then, pure N_2 was flowed and the temperature was increased up to 425 K, until no pyridine was detected in the gas coming out of the cell. The TPD experiment was carried out heating at 12 $K \cdot min^{-1}$, from 425 to 1023 K. Pyridine was detected by a FID detector after methanation [15]. The amount of Brønsted and Lewis acid sites was determined by FTIR analyses of pyridine adsorbed on the samples (Py-IR). Spectral measurements were performed on a JASCO FT-IR 5300 spectrometer equipped with a DTGS detector. The IR spectra were obtained at room temperature after pyridine desorption by evacuation for 1 h at 523, 623 and 673 K.

Chemical state of the metallic species was determined by X-ray Photoelectron Spectroscopy (XPS). It was done in a multitechnique system (SPECS) equipped with a dual Mg/Al X-ray source and a hemispherical PHOIBOS 150 analyzer operating in the fixed analyzer transmission (FAT) mode. The reduced samples were pretreated *in-situ* in H_2/Ar during 10 min at 673 K, and then evacuated at room temperature. Spectra were processed using the software Casa XPS (Casa Software Ltd., UK).

The Mössbauer spectra were obtained in transmission geometry with a 512-channel constant acceleration spectrometer. A source of ^{57}Co in Rh matrix of nominally 50 mCi was used. Velocity calibration was performed against a 12-μm-thick α-Fe foil. All isomer shifts (δ) mentioned in this paper are referred to this standard at room temperature. Temperature was varied between 13 and 298 K working with an ARS closed-cycle cryogenic system. The Mössbauer spectra were fitted using a commercial program with constraints named Recoil [16]. All of them were folded to minimize geometric effects. Samples were analyzed without an *in-situ* reduction.

The amount of carbonaceous materials deposited on the catalysts was determined by Temperature-Programmed Oxidation (TPO) after each reaction test. This analysis was done in a gas stream of 5% (v/v) O_2 in N_2 with a heating rate of 12 $K \cdot min^{-1}$. The oxidation products were detected with a flame ionization detector (FID) after methanation [15].

2.3 Catalytic activity

The catalytic activity was measured at atmospheric pressure in a continuous-flow fixed-bed reactor, made of 5 mm internal diameter quartz tube. Additional details of the reacting system can be found elsewhere [12]. The catalyst was pretreated under flow of H_2 (30 ml·min^{-1}) by heating at 10 K·min^{-1} from room temperature to 773 K. Furfural was fed to the reactor through a saturated H_2/N_2 stream. After each test, the catalyst bed was purged with pure H_2 (30 ml·min^{-1}) at the reaction temperature during 30 min.

The reactor outlet stream was analyzed in a GC (SRI 8610) with a FID detector connected online. The column was an H-1 capillary column (60 m). Standard samples were used in order to identify the reaction products. In addition, a GC–MS (Varian Saturn 2000) equipped with a HP-5 capillary column was used to identify the reaction products collected in a condenser cooled at 273 K.

3. RESULTS AND DISCUSSION

3.1 Catalyst characterization

3.1.1 Surface area and pore size

Table 1 shows the results of surface characterization. The support (SiO_2) presents a BET area of 260 m^2·g^{-1} and a pore volume of 1.08 cm^3·g^{-1}. The adsorption–desorption isotherm (not shown) for pure silica presents a non-pronounced hysteresis loop. This result indicates that there is an important contribution of the external surface to the relatively high value of mesoporous area. The micropores volume is 0.02 cm^3·g^{-1}. The addition of the metals did not significantly modify the BET area and the pore size of the support.

3.1.2 Acidity

The total acid sites density obtained by TPD-Py was 0.061 mol of Pyridine per m^2 of the support. The FTIR analyses of adsorbed pyridine did not show signals at 523 K indicating that the acidity detected by TPD-Py is probably due to weak Brønsted acid sites that do not possess sufficient strength to chemisorb pyridine molecules at 523 K.

3.1.3 X-Ray Diffraction

X-ray diffractograms of mono and bimetallic pre-reduced samples of the catalysts are shown in Figure 1. The X-ray pattern for $Pt_{1.7}$ catalyst shows only the characteristic amorphous SiO_2 shape, indicating that the size of the particles is below the detection limit. The Fe_{15} catalyst shows signals corresponding to α-Fe (JCPDS 6-696) and iron oxides due to their high metallic load. Signals of γ-Fe_2O_3 (JCPD 39-1346) or Fe_3O_4 magnetite (JCPDS 11-614) can be observed. Due to their similarity, these structures are not easy to be distinguished with the XRD technique [17,18]. Therefore, other characterization methods such as Mössbauer and X-ray Photoelectron spectroscopies were used to differentiate the structures of iron oxides. Oxides such as FeO (JCPDS 3-968), α-Fe_2O_3 (JCPDS 33-664) and iron silicates (Fe^{2+}) are not observed in the XRD results. In the case of bimetallic catalysts, no platinum signals are observed either. However, in the case of $Fe_5Pt_{0.5}$ catalyst, the peaks corresponding to α-Fe appear at a lower intensity but at the same 2θ diffraction angles than for Fe_5 sample. This result suggests that the presence of platinum decreases the iron particles size. Table 1 shows the crystal sizes calculated using the Scherrer´s formula based on the main iron peak at 44.71°. In the case of $Fe_7Pt_{0.07}$, the diffractograms was similar to that of the Fe_5 sample, indicating that the effect of Pt on the iron particle size is lower than for higher platinum loads catalysts. No shifts of the 2θ angle signals of iron oxides were observed in the bimetallic catalyst. These results differ with those observed by Pino et al. [10], who studied Pd(1.0)Fe(0.5)/SiO_2 catalysts, and showed shifts in the 2θ angles of Pd crystals. This difference may be due to the very low amount of Pt compared to Fe used in this study. This low Pt/Fe ratio makes it difficult to obtain the diffraction pattern of the alloyed particles.

3.1.4 Temperature Programmed Reduction

Temperature programmed reduction (TPR) profiles of the catalysts studied are shown in Figure 2. The TPR profile for $Pt_{1.7}$ showed two small peaks, the first one at 400 K and the second one at higher temperatures (660-800 K), which are related to the reduction of a PtO_X volumetric phase and highly dispersed particles, respectively [12]. The profile corresponding to Fe_{15} showed two peaks, the first at 653 K and the second one at 850 K approximately. It is a characteristic profile for this type of system with a reduction step around 650 K corresponding to α-$Fe_2O_3 \rightarrow Fe_3O_4$, and the second peak at 850 K that involves several steps, and is as yet under debate which reaction includes. It has been

proposed a sequential reduction ($Fe_3O_4 \rightarrow FeO \rightarrow \alpha$-Fe) and also that these reactions occurs in parallel, with the magnetite being reduced directly to α-Fe and FeO. Differences between Fe_{15} and Fe_5 catalysts are assumed to be due to the large difference in Fe content that leads to an overlapping of the two peaks in the second reduction zone. In the case of $Fe_7Pt_{0.07}$ the first peak of the iron reduction was observed at a lower temperature (603 K), and for the $Fe_5Pt_{0.5}$ catalyst this peak is displayed even at lower temperature (523 K). It can be observed that in the case of the $Fe_5Pt_{0.5}$ the second peak appears at lower temperature than in the case of the $Fe_7Pt_{0.07}$, due to the effect of Pt on the reduction of Fe. Based on these results, catalysts reduction before each reaction was performed at 773 K for an hour for all the catalysts. It was checked that after this treatment no significant reduction peaks were observed, therefore it can be assume that the metals were fully reduced.

3.1.5 Mössbauer Spectroscopy

Mössbauer spectroscopy was used to identify the different iron species and to verify if there is an alloy formation in the bimetallic catalysts. The spectra of the pre-reduced catalysts and their corresponding hyperfine parameters, obtained from the fitting process of the experimental points, are shown in Figure 3 and Table 2, respectively. All spectra were obtained at room temperature.

Fe_{15} catalyst has a sextuplet (green interaction) whose hyperfine parameters (Table 2) are typical of α-Fe [19]. From the ratio of the areas of the different species present in this catalyst, considering the same recoil-free fraction for all of them, a degree of reduction of 81% has been estimated. In addition, two doublets are observed in the central region of the spectrum. The first one (blue interaction) has an isomer shift (δ) typical of Fe^{3+} species, which could be assigned to:

- a superficial layer of γ-Fe_2O_3 produced by the re-oxidation of α-Fe when the catalyst was exposed to air during the sample handling. The production of α-Fe_2O_3 by re-oxidation is dismissed since the formation of this species from α-Fe requires temperatures between 573 and 603 K. These results agree with the X-ray diffractogram where no signals corresponding to α-Fe_2O_3 were observed.
- a fraction of very small oxide particles present in the catalyst precursor, which are not reduced under the conditions used. In this case, they would be superparamagnetic particles of α-Fe_2O_3 [20] produced during the calcination treatment of inorganic iron salts above 623 K.

- paramagnetic Fe^{3+} ions that have diffused into octahedral and/or tetrahedral sites on the surface of SiO_2 during the calcination process.

The quadrupole splitting (Δ), reflects the symmetry of the site in which the Fe^{3+} ions are located. In Fe_{15} this parameter has a very high value in comparison with superparamagnetic iron oxides nanoparticles. As an example, superparamagnetic hematite with sizes between 6 and 17 nm have a constant Δ value of 0.51 ± 0.03 mm/s [21]. Therefore, the assignment of this doublet to paramagnetic Fe^{3+} ions inside octahedral and/or tetrahedral sites on the surface of SiO_2 seems to be the most feasible one. However, examining the X-ray diffractogram and the Mössbauer results together, the presence of superparamagnetic nanoparticles of γ-Fe_2O_3 cannot be discarded due to the appearance of the peak at 2θ=35.45° in the XRD diagram. The doublet corresponding to this species could be overlapped with that assigned to paramagnetic Fe^{3+} ions. As consequence it would be hard to detect. On the other hand, it is possible to affirm that the Mössbauer spectra of these catalysts do not reveal any signal that could belong to Fe_3O_4, neither magnetically blocked [22] nor in a state of superparamagnetic relaxation [23]. For this reason, the presence of Fe_3O_4 can be discarded. Nanoparticles of Fe_3O_4 are quite sensitive to oxygen even at low temperature, resulting in the oxidation to γ-Fe_2O_3 during the drying and preparation of the samples [18]. This could be the origin of this species in the catalyst.

The second doublet (red interaction) has a δ characteristic value of Fe^{2+} ions (Table 2). This has been usually detected in Fe/SiO_2 systems where, during the reduction process with H_2, the diffusion of these ions within the tetrahedral and octahedral sites of the support surface occurs [24, 25]. This process is connected to the enormous stability of the Fe(II) silicates. The ions in the octahedral sites have a greater Δ than those located in tetrahedral sites. Comparing with the Δ values of the bibliography [23, 24] in Fe_{15}, only those ions located in tetrahedral sites are detected. It must be considered that a true silicate compound is not produced. Only a small percentage of the total iron loading is located inside the surface sites of SiO_2. This is coherent with the fact that silicates species were not detected by XRD. Nevertheless, for simplicity this compound is mentioned throughout this work as superficial iron silicate.

The same species were observed in the catalyst Fe_5. The same color assignments for the different interactions were used in Figure 3 for both catalysts, Fe_{15} and Fe_5. The only difference that can be observed is that in the case of the Fe_5 catalyst, Fe^{2+} ions are detected in both types of sites: octahedral (purple curve) and tetrahedral (red curve).

Observing the percentages of these species, it can be seen that their population has practically doubled, which would explain why detection is possible at both sites. The percentage of species that could be assigned to paramagnetic Fe^{3+} ions diffused within SiO_2 has also been doubled. This leads to a significant decrease in the percentage of α-Fe obtained, 58%. In comparison with Fe_{15}, a lower metallic charge leads to a smaller particle size, which generates an increase in the interaction between the oxide and the support, favoring the diffusion of Fe ions into the network of SiO_2. This agrees with XRD diffractograms that shows that Fe_5 has a smaller crystal size than Fe_{15} (Table 1). The lower percentage of iron reduction was corroborated with the TPR area of H_2 consumption. For Fe_5 a smaller total area of H_2 consumption per gram of iron was detected. Besides, the area of the 2nd peak, that is, the reduction zone of the highly dispersed particles with high interaction with the support, represents 79.8% of the total area for Fe_5 and 70.5% for Fe_{15}. This indicates that the proportion of highly disperse particles is greater in the case of Fe_5 compared to Fe_{15}.

In the case of $Fe_5Pt_{0.5}$ (curve IV, Figure 3) it is possible to detect a significant decrease in the hyperfine field of α-Fe (Table 2). Iron-platinum alloys are produced in a wide range of compositions. The most studied ones are $Fe_{60}Pt_{40}$ and $Fe_{50}Pt_{50}$, with special emphasis on the latter due to their particular magnetic properties [26]. Although the Pt/Fe atomic ratio of the $Fe_5Pt_{0.5}$ catalyst is much lower than in these two alloys, a general characteristic observed is that, when an atom of iron has neighboring platinum atoms, its hyperfine field is reduced [26]. Therefore, it is possible to conclude that in this catalyst at least a certain percentage of the platinum is alloyed with iron in the metallic nanoparticles. Other important detail is that this catalyst has the lowest degree of reducibility of the series, 20% of α-Fe, while all the rest have values between 80 and 60%. Comparing the TPR profiles of Fe_{15} and $Fe_5Pt_{0.5}$ shown in Figure 2 it is observed that the first reduction peak (corresponding to the stage $\alpha\text{-}Fe_2O_3 \rightarrow Fe_3O_4$) shifted from 653 K for Fe_{15} to 523 K for $Fe_5Pt_{0.5}$. These results seem contradictory. However, the second peak that represents the reduction to α-Fe has its maximum at 853 K and 909 K in the monometallic and bimetallic catalysts, respectively. Therefore, it could be concluded that the presence of platinum facilitates the first stage of reduction of $\alpha\text{-}Fe_2O_3$ to Fe_3O_4, but hinders the final stage of the reaction $Fe_3O_4 \rightarrow$ α-Fe. In addition, the temperature difference between the two maximums in the TPR profile is larger in the bimetallic catalyst (376 K) compared to the monometallic catalyst (192 K). This fact leads to an increase in the contact time between the Fe_3O_4 and the support, facilitating the migration of Fe ions into the network of the SiO_2.

In other words, the presence of platinum improves the dispersion of the iron particles and, therefore, increases their interaction with the support, producing a lower amount of α-Fe as a final result. This agrees with XRD results and the values of iron crystal sizes shown in Table 1. The iron crystal size for the bimetallic catalyst $Fe_5Pt_{0.5}$ is smaller than the one of the monometallic catalyst Fe_5.

In the case of the catalysts with the ratio Fe/Pt = 100 ($Fe_7Pt_{0.07}$) (curve III, Figure 3), there is no decrease in the hyperfine field of α-Fe of the Mössbauer spectrum, nor in the percentage of reducibility. It is likely that the very small Pt/Fe ratio produces an insignificant quantity of iron atoms with neighboring platinum atoms. Therefore, the decrease of the hyperfine field is not detected. On the other hand, although the first reduction stage is facilitated, the difference in temperature between the first and the second reduction peak in comparison with $Fe_5Pt_{0.5}$ is smaller (329 K). This explains the lower fraction of Fe ions that diffuses into the support network, obtaining a reduction of about 70%. Moreover, by XRD analyses it was observed that the monometallic Fe_5 and the bimetallic $Fe_7Pt_{0.07}$ catalysts have similar iron crystal sizes.

3.1.6 XPS Spectroscopy

The 2p Fe signals of the XPS spectra of pre-reduced iron monometallic catalyst and bimetallic catalysts were analyzed. The percentages of the signals of α-Fe, Fe^{2+} and Fe^{3+} are shown in Table 3. In the case of Fe_{15}, the α-Fe signal percentage is 12.8%, while for $Fe_5Pt_{0.5}$ and $Fe_7Pt_{0.07}$ the values are 3.2% and 9.5%, respectively. These percentages follow the tendencies observed using Mössbauer spectroscopy; however there is a great difference in the absolute values between these techniques. An important difference between these two spectroscopies is that XPS is a surface technique while Mössbauer spectroscopy is a bulk technique. As observed in Mössbauer spectroscopy, the low reduction grade observed by XPS is due to the diffusion of the Fe^{2+} ions into octahedral and/or tetrahedral sites of the surface of SiO_2 during the calcination process. According to the XPS and Mössbauer results, the iron silicates are mainly on the surface of the support while the reduced iron is present as large particles. Therefore, the major part of iron is not observed by the XPS technique, giving as an apparent result a higher proportion of oxidized iron (superficial silicates) relative to the reduced iron (large metal particles) compared to that obtained with Mössbauer spectroscopy.

As mentioned above, it is not easy to distinguish γ-Fe_2O_3 from Fe_3O_4 in XRD patterns because of their similar crystalline structures. On the other hand, spectra of γ-Fe_2O_3 and α-

Fe_2O_3 show very similar patterns in XPS despite their differences in crystal structures [18, 27]. Taking into account that no signals of α-Fe_2O_3 where observed by XRD, the main peak of Fe $2p_{3/2}$ around 711 eV is attributed to Fe^{3+} in γ-Fe_2O_3 and/or Fe^{3+} ions diffused inside the SiO_2 lattice. This assignment is in agreement with Mössbauer spectroscopy. The binding energy of Fe $2p_{3/2}$ around 709 eV could be assigned to the Fe^{2+} component in Fe_3O_4 and/or Fe(II) (superficial silicates). However, Fe_3O_4 was not observed by Mössbauer spectroscopy. In summary, the combination of these two techniques indicates that there is no Fe_3O_4 on these catalysts, and that there is superficial iron silicates formation, favored by Pt and high temperatures.

Table 4 shows the binding energies corresponding to Si 2p and Si 2s signals. A shift of the maximum towards lower values of binding energy is observed as the amount of platinum in the catalyst increases. This is characteristic of the formation of superficial iron silicates and the distortion that iron causes in the structure of silica [28, 29]. There is also a shift of the Si 2p signal for the case of Fe_5 with respect to Fe_{15}, from 103.83 eV to 103.77 eV. Therefore, both the Mössbauer and XPS spectroscopies make it possible to conclude that the lower the iron load the smaller the iron particle sizes, thus increasing the metal-support interaction with more Fe(II) silicates formation.

The Pt 4f XPS spectra for $Pt_{1.7}$ and $Fe_5Pt_{0.5}$ display two and three broads peaks respectively (Supplementary Figure S1), than can be deconvoluted into two pairs of doublets with a spin-orbit splitting of $4f_{7/2}$ and $4f_{5/2}$ states, respectively [30, 31]. Zheng et al. [31] found that the BE of Pt 4f peaks shifts to higher values in the case of an alloy formation between Pt and Fe, indicating a strong interaction between these metals. Similar results were found in the case of Pd-Fe catalyst [7]. Table 5 shows the results of the XPS analyses. It can be observed that the Pt 4f BE is higher in the case of the bimetallic catalyst compared to the monometallic Pt catalyst, indicating that there is an alloy formation between Fe and Pt, in agreement with the results obtained with the Mössbauer spectroscopy.

3.2 Catalytic Activity

High octane compounds with low solubility in water are the desired products for furfural hydrodeoxygenation process. It is also important to achieve reaction paths with no loss of C to avoid a decrease in system efficiency [32]. Among the possible reaction products, furfuryl alcohol, tetrahydrofurfuryl alcohol and tetrahydrofuran are not particularly

suitable as fuel molecules, since they are totally miscible in water [32, 33]. Another possibility of reaction path without ring opening is the production of furan and 2-methylfuran. These compounds have high octane number (RON: 109 and 131 respectively) and low solubility in water. However, furan molecule implies the loss of a C. The complete hydrogenation of the 2-methylfuran must be avoided, since it generates 2-methyltetrahydrofuran (2-MTHF), with a low RON and greater solubility in water [34]. The solubility in water does not exclude a compound from being part of a fuel formulation, as is the case for example of bioethanol addition to gasoline. However, it represents a potential problem since in the presence of a small amount of water in the tank fuel, the compound soluble in water will be extracted from the fuel. Due to its properties, 2-methylfuran has been proposed not only as a simple fuel component but also as a gasoline additive as an octane number booster. Therefore, this research focuses in maximizing the production of 2-methylfuran (2-MF).

The furfural HDO to 2-MF was shown to proceed through furfuryl alcohol as an intermediate. Sitthisa et al. [3] observed that C-O hydrogenolysis over NiFe catalysts is much faster with furfuryl alcohol than with furfural, so they proposed that the path for formation of 2-methylfuran goes through an alcohol intermediate. Vorotnikov et al. [35] used DFT methods on Pd(111) to establish that, although the most preferred path from furfural to 2-MF involves furfuryl alcohol as an intermediate, it can also undergo direct hydrodeoxygenation to 2-MF. Morevover, DFT studies on Mo_2C also showed that a methylfuran-like intermediate is produced after furfural adsorption, suggesting that 2-methylfuran is produced not only from furfuryl alcohol but also directly from furfural [8].

A series of experiments was carried out at different reaction temperatures and the activities and selectivities were analyzed. Before each reaction test, the catalysts were pretreated under H_2 flow at 773 K for 1 h. Then, furfural was fed to the reactor as a saturated H_2/N_2 stream. It has been already established that the order in which the reactants contact the surface is critical. It is fundamental that furfural finds pre-adsorbed atomic hydrogen on the surface to be converted into 2-methylfuran [5]. Our studies determined that the optimum reaction temperature in order to maximize the yield of 2-methylfuran is between 523 K and 573 K for all the catalysts studied.

Figure 4 shows results obtained with different catalysts studied under the same reaction conditions: contact time (catalyst mass (W)/reactants mass flow ($F_{reactant}$)), $W/F_{Furfural}$ = 3 $g_{cat}\cdot h\cdot(g_{furfural})^{-1}$, W/F_{Total} = 0.023 $g_{cat}\cdot h\cdot g^{-1}$, H_2/Furfural molar ratio = 245, T = 573 K. Figure 4 shows that Fe_{15} catalyst was more selective than the $Pt_{1.7}$ one to the

desired products (compare Figures 4A and B). This is due to its lower hydrogenation capacity, with 93% of initial selectivity to 2-MF. The formation of 2-MF occurs by hydrogenation of the C=O bond to the corresponding alcohol (furfuryl alcohol) catalyzed by metal, and then the alcohol dehydration and elimination of oxygen catalyzed by the acidity of the support. This reaction needs only very low acidity. However, iron catalyst presented low stability, showing deactivation during the reaction, decreasing the conversion from 32% to 9%. The catalyst Fe_5 has a performance very similar to Fe_{15}, but with lower conversion, as can be observed in Supplementary Figure S2. On the other hand, $Pt_{1.7}$ catalyst shows a complete conversion of furfural with a high stability, but it has very low selectivity to 2-MF (Figure 4B). Based on these results, Pt-Fe bimetallic catalysts were prepared. The objective was to improve the performance of the catalyst in terms of activity, selectivity and stability, based on the synergistic relationship between these two metals. Two bimetallic catalysts with different Fe-Pt ratio were prepared by co-impregnation technique: $Fe_5Pt_{0.5}$ (Fe/Pt=10) and $Fe_7Pt_{0.07}$ (Fe/Pt=100).

$Fe_5Pt_{0.5}$ catalyst presented 100% of furfural conversion (Figure 4C), being much higher than the one obtained with Fe_{15}. However, there is an increase in the amount of light and fully hydrogenated products such as THF, 2-MTHF and tetrahydrofurfuryl alcohol (THFA) compared to iron monometallic catalysts. Selectivity to 2-MF in this case is low, about 10%.

In the case of the $Fe_7Pt_{0.07}$ catalyst (Figure 4D), although the conversion is lower than in the previous case, it is higher than that obtained with Fe_{15}. In addition, the selectivity to light and fully hydrogenated products is negligible. In summary, $Fe_7Pt_{0.07}$ catalyst has better activity and stability compared to the iron monometallic catalyst, and better selectivity to 2-MF compared to the monometallic $Pt_{1.7}$ and the bimetallic $Fe_5Pt_{0.5}$ catalysts. The deactivation of the $Fe_7Pt_{0.07}$ catalyst is less pronounced than in the case of the Fe_{15} catalyst, reaching a pseudo-steady state conversion at 160 min of reaction. This is attributed to the equilibrium between formation of deactivating species and the hydrocracking of the coke precursors [36]. It was reported that at low platinum loadings, particles of sizes less than 2 nm are highly selective towards decarboxylation, while particles larger than 2 nm predominantly produce furfuryl alcohol, which is an intermediate compound to obtain 2-methylfuran [37]. However, in this case, in combination with iron particles these products were not observed. Then, the best production of 2-MF is obtained with $Fe_7Pt_{0.07}$ catalyst.

In conclusion, the catalyst $Fe_7Pt_{0.07}$, ratio Fe/Pt = 100, is the one that presents the best properties for the purposes of this work.

To test the hypothesis for the promoting effect of the bimetallic catalysts, a physical mixture of Pt/SiO_2 and Fe/SiO_2 was used in the conversion of furfural (Supplementary Figure S3). The mixture was prepared maintaining the proportion of Pt and Fe that has the $Fe_7Pt_{0.07}$ catalyst. The mixture shows more conversion but also much higher selectivity to light products in comparison to the bimetallic catalyst $Fe_7Pt_{0.07}$. Actually, it behavior was similar to the platinum monometallic catalyst. These results, together with the characterization techniques, demonstrate that the bimetallic catalyst has a better catalytic performance due to the synergic effect between Pt and Fe. A similar comparison was made by other authors to evaluate the effect of the addition of Fe to Pd or Ni catalysts [3, 7].

3.2.1 Coke deposits: deactivation mechanism.

In this section, the amount of coke deposited in each catalyst is studied and correlated with the presence of different coke precursors formed along the reactor. To do this, information regarding the reaction mechanism for furfural hydrodeoxygenation already reported is used.

Activity, selectivity to the different products, and coke deposits were analyzed for each catalyst as a function of reaction temperature (523 to 573 K). Coke amount deposited on each catalyst and its combustion profile as a function of temperature were obtained by temperature programmed oxidation analyses (TPO). The results of coke contents on the catalysts are shown in Table 6.

The monometallic iron catalyst (Fe_{15}) presents a large amount of coke that explains the rapid loss of activity. Table 6 shows that at 550 K the conversion and 2-MF yield are higher than at 523 and 573, and also that the amount of coke is higher at this intermediate temperature. The differences in conversion are due to the different deactivation rates that occur during the first 20 min of reaction. It has to be kept in mind that the activity data reported in Table 6 correspond to samples taken at a time on oil of 20 min, and that the coke content was measured after a reaction of 6 h. The amount of coke deposited on a given catalyst is a complex function of the reaction temperature, because this variable affects the relative rates of the different reaction steps involved in the mechanism, and the relative rates of oligomerization-cracking-dehydrogenation of the coke precursors, leading in each case to carbon deposits with different toxicities. This means that a given amount

of coke can deactivate the catalyst in different ways depending upon the reaction conditions. For example, it has been shown that in alkylation catalysts, a very small amount of coke formed at high temperature is much more toxic than a larger amount of coke formed at lower temperatures [38]. Figure S4 (Supplementary Material) shows the activity data obtained at 550 K, maintaining the other conditions used in Figure 4. At both temperatures, the main product was 2-MF, with a conversion at 20 min of 32% at 573 K, and 40% at 550 K. A significant difference is that light hydrocarbons appear among the products at 550 K, while these compounds are not observed at 573 K. The higher C-C bond scission activity maintained at 550 K might be the reason of the lower amount of coke deposited at this temperature. Therefore, it can be concluded that there is a complex relationship between activity, deactivation and the reaction temperature, and that a higher amount of coke not necessarily leads to a more pronounced deactivation.

Figure 5A shows TPO profiles of Fe_{15} after reactions at different temperatures. It is observed that coke, independently of the total amount, burns more easily as the reaction temperature at which it is deposited decreases. Usually this behavior is related to different H/C ratios in the coke: as this ratio increases, the coke oxidation temperature decreases. The typical behavior is that as the reaction temperature increases, coke becomes more dehydrogenated and difficult to be burnt out.

In order to obtain more information regarding the coke precursors, different reaction experiments were carried out at 573 K separating the catalyst bed in 3 parts, using quartz wool between adjacent beds. After reaction, the coke content of each bed was analyzed by TPO. Table 7 shows the percentages of carbonaceous deposits in each portion of the Fe_{15} and $Fe_7Pt_{0.07}$ catalysts beds when furfural, 2-MF or furan was individually fed as reagent at 573 K. The amount of coke deposited on Fe_{15} was significantly higher when feeding furfural, being the coke formation negligible when the reactants were 2-MF or furan. On the other hand, the amount of coke in the inlet portion of the bed is higher than in the outlet portion when the reactant is furfural. This molecule is mainly converted to furan and 2-MF. Therefore, in the 3rd fraction of the catalytic bed mostly 2-MF and furan are present. As a consequence, the largest amount of coke is concentrated in the first part of the bed since there is the highest concentration of furfural. At the end of the bed, there is a low amount of coke because the furan and 2-MF are the main compounds in this section, and these compounds do not form coke in quantities as high as furfural, as can be seen in Table 7. These results show that the coking mechanism is a parallel type, with the coke being formed mainly from furfural. As catalyst deactivates, mainly in the reactor inlet,

higher concentration of furfural reaches the reactor outlet increasing the coke deposition in this portion of the bed. The maximum peak of coke combustion is at 665 K (TPO profile not shown). The test carried out with the iron catalyst bed divided in 3 parts feeding 2-MF showed that furan (selectivity 70%), light compounds and butanol (selectivity 25%) were the main products. Butanol is formed as a consequence of the hydrogenation of furan and the opening of the tetrahydrofuran ring [39, 40]. The maximum coke combustion peak was at 720 K. Although the amount of coke was very low, it was higher in the inlet than in the outlet of the bed, indicating that 2-MF is a precursor of coke, but does not lead to a fast coke deposition. The obtained coke is even more difficult to burn than that obtained when feeding furfural as reagent. Finally, the same experience (3 beds) was carried out feeding furan to the system. In this case, less coke is obtained at the reactor inlet bed than at the outlet bed, indicating that furan forms less coke than its products (see Table 7). The TPO profile (not shown) shows that an important part of the carbonaceous deposits burns at 390 K and other part at 550 K. Tetrahydrofuran (THF) was the main product (selectivity 58%) but also molecules that are formed from its ring opening like n-butanol (selectivity 13%), and other light compounds (selectivity 29%) were observed as products. Indeed, the production of THF from furfural was reported to generate high yield of coke during the process [41]. This coke has high carbon content and is deficient in hydrogen.

There are several mechanisms of coke formation. Furfural molecule is adsorbed on the iron particles preferably through the O of the C=O group, as it was revealed by DFT studies. Sittisa et al. [3] established that there is a strong interaction between the carbonyl O and the oxyphilic Fe atoms on the surface. This favors the formation of coke precursors and products, mainly furan and 2-MF. The latter also forms coke precursors and hydrogenated and light compounds. In conclusion, in the presence of iron particles, the reaction of furfural conversion to 2-MF is favored, being furfural the main source of coke precursors. Scheme 1 shows the proposed coke formation path. It is important to recall, that Mössbauer spectroscopy showed that the proportion of α-Fe was the highest in the case of the Fe_{15}, and therefore it has high selectivity to 2-MF and coke formation.

The platinum catalyst giving a conversion of 100% under reaction conditions of Figure 4, presented less amount of coke deposited on its surface than the iron catalyst, as shown in Figure 6 and Tables 6 and 8. The TPO profile of Figure 6 for this catalyst shows a peak at low temperature, which is related to the combustion of coke deposited on the metal particles and surroundings. The coke that burns at the highest temperature (473-773 K) corresponds to the coke deposited on the support [42-44]. This type of profile had already

been observed in catalysts used in reactions with other model molecules [45]. It was reported that the formation of carbonaceous deposits from furfural are favored at 377-385 K on Pt catalysts [5]. In our case, this is probably mitigated because of the higher operation temperature. As it is known, the furfural molecules are adsorbed on the platinum particles preferably through the furanic ring, forming a large amount of light and hydrogenated compounds. The greater interaction of the molecule with the surface of the catalyst in comparison with iron catalyst favors the carbon-carbon bond scission reactions and therefore generates less amount of coke. On the other hand, the platinum particles generate a hydrogen *spillover* that increases the amount of available hydrogen atoms producing a significant improvement in the stability of the catalyst.

This catalyst has 100% selectivity to light compounds at 573 K as shown in Table 6. At this temperature carbon-carbon bond scission is favored. At 550 K, lower yield to light compounds and higher selectivity at 2-MF are obtained. At 523 K, the highest furan yield is achieved and hydrogenation reactions are favored, so the highest amount of 2-MTHF is obtained. The amount of coke deposited decreases as the reaction temperature increases, because the carbon-carbon bond scission capacity of platinum increases with temperature, thus reducing the concentration of coke precursors on the catalyst surface

The amount of coke on iron monometallic catalyst passes through a maximum at a reaction temperature of 550 K, while on the platinum monometallic catalyst the coke content decreases as the reaction temperature increases.

When platinum is incorporated in the formulation with a ratio of Fe/Pt = 10 ($Fe_5Pt_{0.5}$), the amount of coke follows the trend of the platinum monometallic catalyst: the higher the reaction temperature the lower the amount of coke (Table 6). In addition, the amount of coke is similar in these two catalysts and is lower than in the Fe_{15} catalyst. Therefore the presence of Pt in the formulation leads to lower deactivation because the furfural, which is the main coke precursor, is rapidly converted to other products. There are important changes that occur on the Fe catalyst when Pt is added. One of them is that the amount of α-Fe on the catalyst surface decreases. Another change is that an alloy Fe-Pt is formed, modifying the electronic structure of Fe and Pt and consequently the strength of the furfural and other oxygenated compounds adsorption. The dissociation of hydrogen on the Pt atoms favors the hydrogenation of the O atom in the C=O bond. These changes improve the stability making it possible to have good conversion, although the selectivity to the desired products is yet not comparable to that of Fe. The selectivity to 2-MF + furan is lower in this bimetallic catalyst than with Fe_{15} at all the temperatures used in this study.

Bimetallic catalyst $Fe_7Pt_{0.07}$ shows better stability than the Fe_{15} catalyst, and higher selectivity to 2-MF than the $Fe_5Pt_{0.5}$ catalyst (see Table 6). A pseudo-steady conversion was observed after 160 min (Figure 4D), indicating that the coke formation rate is equalized with the hydrocracking of its precursors [36]. The amount of coke decreases when conversion and reaction temperature increases. However, the TPO profiles show that coke burns more easily when the reaction temperature decreases, despite being in higher quantity, as seen in Figure 5B.

Catalytic tests were carried out with 3 consecutive beds of $Fe_7Pt_{0.07}$ using furfural, 2-MF and furan as reagents, similarly to the experiments carried out with Fe_{15}. The results of the percentages of coke in each bed portion are shown in Table 7. The maximum peak of coke combustion was at 633 K when furfural was the reactant. Furfural, the products (methylfuran and tetrahydrofuran) and also CO formed from decarboxylation of furfural to furan, may be responsible for carbon deposits on the catalytic surface at low temperatures [5].

When 2-MF was used as reagent, more coke was formed in the inlet bed than in the outlet, indicating that 2-MF is a more important coke precursor than the products formed along the bed (see Table 7). However, the amount of coke deposited in this case is an order of magnitude lower than that deposited from furfural. Furan, light compounds and butanol were the main products. $Fe_7Pt_{0.07}$ presented 60% of selectivity to butanol and 31% to furan. The maximum coke combustion peak was at 718 K. When the furan molecule was the reactant over $Fe_7Pt_{0.07}$ catalyst, less coke was obtained at the reactor inlet than at the outlet as shown in Table 7, which is the same coke profile along the bed as in the case of the Fe_{15}. This indicates that furan forms less coke than its products. The maximum in the TPO profile was displayed at 543 K. Light compounds, THF and butanol were the main products. In this case, 60% of selectivity to light compounds, 20.4% to THF and 19.8% to butanol were obtained. As it was already commented, THF was reported to generate high yield of coke [41].

The addition of Pt in this very low proportion (0.07 wt%) is enough to decrease the coke values with respect to monometallic Fe catalysts in all experiments.

Figure 6 shows the TPO profiles and in Table 8 the corresponding values of carbonaceous deposits of all catalysts used at the same reaction conditions (conversion and selectivity reaction results shown in Figure 4). The incorporation of platinum to the iron catalyst implies an increase in the stability of the catalyst precisely because of the platinum's ability to break bonds of the coke precursor molecules. The decrease of the

total amount of coke deposited and a shift of the combustion peaks towards lower temperatures is observed (Figure 6). The presence of platinum, even in very low proportions, changes the relative speeds of the reactions involved in this system, but on the other hand it generates a hydrogen spillover that leads to an important improvement in the stability of the catalyst.

However, the incorporation of an excessive amount of platinum should be avoided, not only because it generates light products but also because it decreases the size of the iron particles, increasing their interaction with the support (formation of superficial silicates) and therefore decreasing the amount of iron available for the reaction.

That is, the ratio Fe/Pt ratio in the surface regulates the amount of coke deposited because it modifies the iron particle sizes, the interaction with the support and the amount of hydrogen available for the reactions, altering the reaction and coke formation mechanisms.

3.2.2 Hydrogen Effect

Another variable studied was the relative amount of H_2 in the system. In this work, the conversion of furfural and selectivity to the different products were evaluated using Fe_{15} catalyst at W/F = 3 g_{cat} h $g_{furfural}^{-1}$ varying the H_2/Furfural ratio (600, 300 and 100). Results are shown in Figure 7. As expected, this ratio significantly affects the activity of the catalyst, not only because the H_2 is a reagent, but also due to its inhibition effect in the formation of undesirable heavy products. This fact is shown in the study of deoxygenation of esters with Pt/Al_2O_3 [46] and was observed in other studies [13, 14, 45]. Taylor et al. [5] studied the influence of H/furfural ratio on platinum catalyst by temperature-programmed reaction spectrometry (TPRS) and scanning tunneling microscopy (STM). Furfural's adsorption and hydrogenation over Pt(111) was analyzed. It was found that at high H(a):furfural ratio on the surface, the stepwise hydrogenation of furfural to furfuryl alcohol, and its subsequent HDO to methyl furan, was favored. At a low H(a):furfural ratio on the surface, insufficient hydrogen is available to further hydrogenate the furfuryl alcohol, which hence becomes the dominant product; however, in the latter scenario, more furfural desorbs molecularly. Therefore, as also observed in this work, furfural conversion diminished when surface H(a):furfural ratio is reduced.

The monometallic iron catalyst does not show the same behavior as regards 2-MF selectivity. At high H_2/Furfural ratio, a high selectivity to furan is obtained with Fe_{15} catalyst

(Figure 7A). However, in spite of a high H_2/Furfural ratio the monometallic Fe_{15} catalyst rapidly deactivates. Higher values of H_2/Furfural ratio leads to higher conversion. Figure 4 shows that as the Fe/Pt ratio increases, lower conversion are obtained and 2-MF selectivity increased (compare Figure 4C ($Fe_5Pt_{0.5}$) with Figure 4D ($Fe_7Pt_{0.07}$)). Similar behavior is observed in Figure 7, when changing the H_2/Furfural ratio with the Fe_{15} catalyst. As this variable decreases, a faster deactivation of Fe_{15} occurs. It is important to highlight, that 2-MF selectivity is higher at higher H_2/Furfural ratio, as can be concluded comparing Figures 7 A, B and C.

Moreover, in an experiment the H_2/Furfural ratio was increased from 100 to 300 at a certain moment, keeping the other parameters constant. When the partial pressure of H_2 increases, a significant recovery of the activity and the 2-MF selectivity occurred, as shown in Supplementary Figure S5. This agrees with the results of Figure 7, and shows that after the Fe is partially deactivated, a higher H_2/Furfural ratio leads to higher 2-MF selectivity.

These results have an important consequence in process design. According to this analysis, the reaction should be started with a low H_2/Furfural ratio, and gradually increases this variable as the catalyst deactivates, making it possible to optimize the selectivity to 2-MF during the reaction.

3.3 Catalyst regeneration

Several reaction-regeneration cycles were carried out with the Fe_{15} catalyst. The first regeneration treatment was carried out with hydrogen at 773 K and the others with air at the reaction temperature (573 K). After each regeneration treatment, the reaction was repeated under the same initial conditions. Reaction temperature, W/F and H_2/furfural ratio used in this case were 573 K, 3 $g_{cat}\cdot h\cdot(g_{furfural})^{-1}$ and 600 respectively. These values were chosen in order to have significant deactivation. Figure 8A shows the results of conversion and yields to different products before and after each treatment. After regeneration with hydrogen at 773 K, the activity is recovered by 71%. However, the selectivity remains constant. After regeneration with air at 573 K, the activity recovers completely to the initial value of the experiment. The 2-MF selectivity does not change after the different treatments. In a second experiment the Fe_{15} catalyst was regenerated with air at 773 K. The values of W/F and H_2/Furfural ratio were chosen in order to have significant deactivation, W/F= 5 $g_{cat}\cdot h\cdot(g_{furfural})^{-1}$, molar ratio H_2/Furfural = 800, reaction temperature = 573 K. As shown in Supplementary Figure S6, the activity is partially recovered, although

the 2-MF selectivity is maintained. The regeneration at 773 K leads to the formation of light compounds in the second reaction cycle. Since in the first cycle there was not production of these compounds, it can be concluded that the regeneration in air at 773 K induced a segregation of Pt from Fe, having as a consequence higher conversion to products via C-C bond scission.

The same regeneration study was made with the $Fe_7Pt_{0.07}$ catalyst. The results are shown in Figure 8B. As in the case of Fe_{15}, these values were chosen in order to have a significant deactivation (reaction temperature 550 K, W/F = 1.25 $g_{cat}\cdot h\cdot(g_{furfural})^{-1}$, molar ratio H_2/Furfural = 168). After each regeneration treatment, the reaction was repeated under the same initial conditions. An initial treatment with H_2 at 773 K for 1 h was carried out after 136 min of reaction. Then several regeneration-reaction cycles were carried out with air at 550K. In this case, the catalytic activity (conversion and selectivity) after the regeneration with H_2 at 773 K was partially recovered. It was possible to obtain a conversion equal to 85% of the initial value obtained in the first reaction cycle, which is a higher value than that obtained with the iron catalyst for this same treatment. No significant selectivity changes were observed due to regeneration, keeping 2-MF as the main product after burning the carbonaceous residue. However, regeneration with H_2 produced a small increase in the 2-MF/light compounds ratio. The second regeneration cycle was carried out with air at 550 K (reaction temperature). In this case it was possible to recover 100% of the initial activity of the catalyst. Furthermore, the treatment with air improved the activity of the catalyst, and consequently the selectivity to 2-MF, which decreases with the deactivation of the catalyst. The second regeneration with air recovers the activity by 97%. It decreases the selectivity to 2-MF and furan and increases the selectivity to light compounds, significantly decreasing the 2-MF/light products ratio. After the 3rd cycle of regeneration with air, the activity recovers 95% with respect to the first cycle of regeneration with air but the selectivities to the products remain similar. The production of light compounds observed in these experiments was not expected. It has to be emphasized that results shown in Figure 8B were obtained at 550 K. These results suggests that the successive oxidation/reduction cycles may lead to a phase segregation, with Pt being separated at least in a low proportion, thus increasing the initial conversion and the production of light compounds.

There is an important conclusion that can be obtained from these results, which is that the $Fe_7Pt_{0.07}$ catalyst can be regenerated without decreasing the selectivity to 2-MF.

4. Conclusions

The gas phase conversion of furfural in the presence of iron particles on silica is highly selective to 2-methylfuran at 573 K. However, Fe/SiO_2 presented very low stability. Not only furfural but several products are responsible for carbon deposition on the catalytic surface. However, furfural is the most important coke precursor and because of this, a parallel-type mechanism for coke formation takes place. The coke deposition from furan and 2-MF is one tenth approximately as compared to that formed from furfural. Adding a second metal like platinum, even in very low proportions, generates a hydrogen spillover leading to an important improvement in the stability of the catalyst. On the other hand, it implies a change in the relative speeds of the reactions involved in this system. The fastest conversion of furfural in the presence of Pt, forming compounds that form lower amounts of coke is one of the reasons of the higher stability of the bimetallic catalysts. However, the incorporation of an excessive amount of platinum should be avoided, because not only it generates undesirable products but also because it produces a segregation of the iron particles, decreasing the amount of iron available for the reaction. The observed behavior is explained in terms of a reduction of the iron particles size, and the consequent increase of their interaction with the support (formation of superficial silicates), induced by the presence of platinum as evidenced by XPS, XRD, and Mössbauer spectroscopy characterization. Also, it is demonstrated that in these catalysts, an alloy formation Fe-Pt takes place. The catalyst $Fe_7Pt_{0.07}$ shows a synergistic effect between the two metals, making it possible to obtain 2-MF with good selectivity and stability.

Therefore, the Fe/Pt ratio in the surface regulates the amount of coke deposited because it modifies the iron particle sizes, the interaction with the support and the amount of hydrogen available for the reactions, altering the reaction and coke formation mechanisms.

Moreover, regeneration of the studied monometallic and bimetallic catalysts is possible with air at the reaction temperature. The regeneration temperature should not be too high, to avoid the segregation of Pt, thus decreasing the catalytic performance for excessive formation of light compounds.

Acknowledgments

The authors wish to acknowledge the financial support received from ANPCyT (PICT 2016-1307), CONICET-FYPF (PIO 2013), and UNL (CAID 2016

504201501000046LI). Thanks are also given to Claudio Perezlindo and Pablo Ilari for the technical support.

References

[1] J.P. Lange, E. Van Der Heide, J. van Buijtenen, R. Price, Chem Sus Chem 5 (2012) 150-166. https://doi.org/10.1002/cssc.201100648.

[2] M. Ershov, E. Grigor'eva, A. Guseva, N.Y. Vinogradova, D. Potanin, V. Dorokhov, P. Nikul'shin, K. Ovchinnikov, Russ. J. Appl. Chem. 90 (2017) 1402-1411. https://doi.org/10.1134/S1070427217090051.

[3] S. Sitthisa, W. An, D.E. Resasco, J. Catal. 284 (2011) 90-101. https://doi.org/10.1016/j.jcat.2011.09.005.

[4] C. Wang, J. Luo, V. Liao, J.D. Lee, T.M. Onn, C.B. Murray, R.J. Gorte, Catal. Today 302 (2018) 73-79. https://doi.org/10.1016/j.cattod.2017.06.042.

[5] M.J. Taylor, L. Jiang, J. Reichert, A.C. Papageorgiou, S.K. Beaumont, K. Wilson, A.F. Lee, J.V. Barth, G. Kyriakou, J. Phys. Chem. C. 121 (2017) 8490-8497. https://doi.org/10.1021/acs.jpcc.7b01744.

[6] B.M. Reddy, G.K. Reddy, K.N. Rao, A. Khan, I. Ganesh, J. Mol. Catal. A Chem. 265 (2007) 276-282. https://doi.org/10.1016/j.molcata.2006.10.034.

[7] S. Xu . X. Yan . Q. Bu . H. Xia. Cellullose 24 (2017) 2403-2413 https://doi.org/10.1007/s10570-017-1275-0

[8] K. Xiong, W. S. Lee, A. Bhan, J. G. Chen. ChemSusChem. 7 (2014) 2146-2151 https://doi.org/10.1002/cssc.201402033

[9] S. Sitthisa, T. Pham, T. Prasomsri, T. Sooknoi, R.G. Mallinson, D.E. Resasco, J. Catal. 280 (2011) 17-27. https://doi.org/10.1016/j.jcat.2011.02.006.

[10] N. Pino, S. Sitthisa, Q. Tan, T. Souza, D. López, D.E. Resasco, J. Catal. 350 (2017) 30-40. https://doi.org/10.1016/j.jcat.2017.03.016.

[11] F. Wang, Z. Zhang, ACS Sustainable Chem. Eng. 5 (2017) 942−947. https://doi.org/10.1021/acssuschemeng.6b02272

[12] M. Zanuttini, C.D. Lago, C.A. Querini, M.A. Peralta, Catal. Today. 213 (2013) 9-17. https://doi.org/10.1016/j.cattod.2013.04.011.

[13] M. Zanuttini, B. Dalla Costa, C. Querini, M. Peralta, Appl. Catal. A. 482 (2014) 352-361. https://doi.org/10.1016/j.apcata.2014.06.015.

[14] M. Zanuttini, C. Lago, M. Gross, M. Peralta, C. Querini, Ind. Eng. Chem. Res. 56 (2017) 6419-6431. https://pubs.acs.org/doi/10.1021/acs.iecr.7b00521.

[152] S. Fung, C. Querini, J. Catal. 138 (1992) 240-254. https://doi.org/10.1016/0021-9517(92)90020-I.

[16] K. Lagarec, D. Rancourt, Mössbauer Spectral Analysis Software, Version 1.0. Department of Physics, University of Ottawa, 1998.

[17] Y. Zhu, F. Jiang, K. Chen, F. Kang, Z. Tang, J. Alloy Compd 509 (2011) 8549-8553. https://doi.org/10.1016/j.jallcom.2011.05.115.

[18] H. Cui, Y. Liu, W. Ren, Ad. Powder Technol. 24 (2013) 93-97. https://doi.org/10.1016/j.apt.2012.03.001.

[19] R. Preston, S. Hanna, J. Heberle, Phys. Rev. 128 (1962) 2207. https://doi.org/10.1103/PhysRev.128.2207.

[20] S. Mørup, M.F. Hansen. H. Kronmüller and S. Parkin (Eds) Handbook of Magnetism and Advanced Magnetic Materials. Volume 4: Novel Materials, 2007.

[21] F. Bødker, S. Mørup. Europhys. Lett., 52 (2) (2000) 217–223. https://iopscience.iop.org/article/10.1209/epl/i2000-00426-2/pdf

[22] R. Vandenberghe, E. De Grave, C. Landuydt, L. Bowen, Hyperfine Interact. 53 (1990) 175-195. https://doi.org/10.1007/BF02101046.

[23] D. Rancourt, J. Daniels, Phys. Rev. B 29 (1984) 2410. https://doi.org/10.1103/PhysRevB.29.2410.

[24] B.S. Clausen, H. Topsøe, S. Mørup, Appl. Catal. 48 (1989) 327-340. https://doi.org/10.1016/S0166-9834(00)82802-X.

[25] I.O.P. De Berti, J.F. Bengoa, S.J. Stewart, M.V. Cagnoli, G. Pecchi, S.G. Marchetti, J. Catal. 335 (2016) 36-46. https://doi.org/10.1016/j.jcat.2015.12.004.

[26] T. Goto, H. Utsugi, K. Watanabe, Hyperfine Interact. 54 (1990) 539-544. https://doi.org/10.1007/BF02396086.

[27] T.d. Fujii, F. De Groot, G. Sawatzky, F. Voogt, T. Hibma, K. Okada, Phys. Rev. B. 59 (1999) 3195. https://doi.org/10.1103/PhysRevB.59.3195.

[28] C. Wagner, D. Passoja, H. Hillery, T. Kinisky, H. Six, W. Jansen, J. Taylor, J. Vac. Sci. Technol. 21 (1982) 933-944. https://doi.org/10.1116/1.571870.

[29] B. Ali, F. Ghafoor, M.I. Shahzad, S.K. Shah, S.M. Abbas, J. Power Sources. 396 (2018) 467-475. https://doi.org/10.1016/j.jpowsour.2018.06.049.

[30] K. Shuklaa, R.K. Ramana, N.A. Choudhurya, K.R. Priolkarb, P.R. Sarodeb, S. Emurac, R. Kumashiro, J. Electroanal. Chem. 563 (2004) 181–190. https://doi.org/10.1016/j.jelechem.2003.09.010

[31] FS Zheng, SH Liu , CW Kuo Int. J. Hydrog. Energy 41 (2016) 2487-2497 https://doi.org/10.1016/j.ijhydene.2015.12.018

[32] T. Wallner, A. Ickes, K. Lawyer, Proceedings of the FISITA 2012 World Automotive Congress, Springer, 2013, pp. 15-26.

[33] D.E. Resasco, S. Sitthisa, J. Faria, T. Prasomsri, A.J.F. Albanese, M.P. Ruiz (Eds) Solid Waste as a Renewable Resource: Methodologies, 2011, pp. 103-144.

[34] E. Christensen, J. Yanowitz, M. Ratcliff, R. L. McCormick. Energ. Fuel. 25 (10) (2011) 4723-4733. https://doi.org/10.1021/ef2010089.

[35] V. Vorotnikov, G. Mpourmpakis, D. G. Vlachos, ACS Catal. 2 (2012) 2496-254 https://doi.org/10.1021/cs300395a

[36] T. Cordero-Lanzac, R. Palos, I. Hita, J.M. Arandes, J. Rodríguez-Mirasol, T. Cordero, P. Castaño. Appl. Catal. B 239 (2018) 513-524. https://doi.org/10.1016/j.apcatb.2018.07.073

[37] V.V. Pushkarev, N. Musselwhite, K. An, S. Alayoglu, G.A. Somorjai, Nano lett. 12 (2012) 5196-5201. https://doi.org/10.1021/nl3023127.

[38] C.A. Querini. Cat. Today. 62 (2000) 135-143. https://doi.org/10.1016/S0920-5861(00)00415-6.

[39] J. Kijeński, P. Winiarek, T. Paryjczak, A.Lewicki, A. Mikołajska. Appl. Catal. A. 233 (1-2) (2002) 171-182. https://doi.org/10.1016/S0926-860X(02)00140-0

[40] S. Sitthisa, D. E. Resasco. Catal. Lett. 141 (6) (2011) 784-791. https://doi.org/10.1007%2Fs10562-011-0581-7

[41] K. Yan, G. Wu, T. Lafleur, C. Jarvis. Renew. Sust. Energ Rev., 38 (2014) 663-676. https://doi.org/10.1016/j.rser.2014.07.003

[42] J. Barbier, E. Churin, J. Parera, J. Riviere, React. Kinet. Catal. Lett. 29 (1985) 323-330. https://doi.org/10.1007/BF02068522.

[43] J. Barbier, Coking of reforming catalysts, Studies in Surface Science and Catalysis. Elsevier, 1987, pp. 1-19.

[44] J. Barbier, E. Churin, P. Marecot, J. Catal. 126 (1990) 228-234. https://doi.org/10.1016/0021-9517(90)90061-N.

[45] M.S. Zanuttini, M.A. Peralta, C.A. Querini, Ind. Eng. Chem. Res. 54 (2015) 4929-4939. https://doi.org/10.1021/acs.iecr.5b00305

[46] P.T. Do, M. Chiappero, L.L. Lobban, D.E. Resasco, Catal. lett. 130 (2009) 9-18. https://doi.org/10.1007/s10562-009-9900-7.

Tables

Table 1: BET surface, total pore volume, micropore volume, and average pore diameter (Dp) values for the fresh reduced catalysts, and crystal size obtained by XRD.

Catalyst	BET Area ($m^2.g^{-1}$)	Total Pore Volume ($cm^3.g^{-1}$)	Micropore Volume ($cm^3.g^{-1}$)	Average Pore Diameter (nm)	Lc Fe (DRX) (nm)
Fe_{15}	205	0.81	0.008	15.8	25
Fe_5	212	0.89	0.012	16.8	13
$Fe_5Pt_{0.5}$	230	0.96	0.010	16.6	9
$Fe_7Pt_{0.07}$	226	0.94	0.013	16.5	12
$Pt_{1.7}$	251	1.04	0.012	16.6	

Table 2: Hyperfine Mössbauer parameters for the catalysts obtained at 298 K.

Species	Parameters	Fe_{15}	Fe_5	$Fe_5Pt_{0.5}$	$Fe_7Pt_{0.07}$
α-Fe	H (kG)	330.7 ± 0.3	330.9 ± 0.5	321 ± 5	331.3 ± 0.8
	δ (mm/s)	0.01 ± 0.01	0.01 ± 0.01	-0.04 ± 0.07	0.01 ± 0.01
	2ε (mm/s)	0.01 ± 0.01	0.01 ± 0.01	-0.1 ± 0.1	-0.01 ± 0.02
	%	81 ± 1	58 ± 2	19 ± 4	67 ± 3
SP iron oxide and/or paramagnetic Fe^{3+}	Δ (mm/s)	1.11 ± 0.05	0.88 ± 0.03	0.82 ± 0.05	0.87 ± 0.08
	δ (mm/s)	0.21 ± 0.03	0.22 ± 0.03	0.18 ± 0.05	0.25 ± 0.06
	%	10 ± 1	20 ± 2	34 ± 5	14 ± 3
Fe^{2+} inside of SiO_2 octahedral sites	Δ (mm/s)	-----	2.4 ± 0.1	2.4 ± 0.2	2.5 ± 0.2
	δ (mm/s)	-----	0.52 ± 0.05	0.48 ± 0.09	0.45 ± 0.09
	%	-----	7 ± 1	10 ± 3	7 ± 2
Fe^{2+} inside of SiO_2 tetrahedral sites	Δ (mm/s)	1.11 ± 0.05	0.92 ± 0.04	0.89 ± 0.05	1.0 ± 0.1
	δ (mm/s)	0.67 ± 0.03	0.60 ± 0.03	0.52 ± 0.04	0.66 ± 0.07
	%	9 ± 1	15 ± 2	37 ± 5	12 ± 3

H: hyperfine magnetic field; δ: isomer shift (all isomer shifts are referred to α-Fe at 298K); 2ε: quadrupole shift; Δ: quadrupole splitting; SP: superparamagnetic species.

Table 3: XPS results. Fe2p signals.

Fe2p		Catalyst			
		Fe_{15}	Fe_5	$Fe_5Pt_{0.5}$	$Fe_7Pt_{0.07}$
%	Fe^0	12.8	3.4	3.2	9.5
	Fe^{2+}	56.1	49.1	71.5	61.0
	Fe^{3+}	31.1	47.5	25.3	29.5

Table 4: XPS results. Si 2p and Si 2s signals.

Catalyst	Si 2p (eV)	Si 2s (eV)
SiO_2	103.85	154.79
Fe_{15}	103.83	154.77
Fe_5	103.77	154.78
$Fe_7Pt_{0.07}$	103.73	154.75
$Fe_5Pt_{0.5}$	103.59	154.55

Table 5: Binding energies and relative contents of metallic Pt and PtOx determined from Pt 4f XPS spectra**.**

Catalyst	Fe/Pt ratio	Relative Intensities		Binding Energy (BE) (eV)			
				Pt^0		PtO_x	
		Pt^o	PtOx	Pt 4 $f_{7/2}$	Pt 4 $f_{5/2}$	Pt 4 $f_{7/2}$	Pt 4 $f_{5/2}$
Pt(1.7)	0	53,5	46,5	70.30	73.80	72.00	75.05
Fe(5)Pt(0.5)	10	76,5	23,5	70.60	74.30	73.20	78.20

Table 6: Reaction activity and selectivity after 20 min of reaction test and the formation of carbonaceous deposits as a function of the reaction temperatures, $W/F_{furfural}$ = 3, W/F_{total} = 0.023, H_2/Furfural = 245.

Catalyst	T (K)	Xi (%)	$S_{2\text{-MF}}$ (%)	S_F (%)	$S_{2\text{-MTHF}}$ (%)	S_{LHC}[a] (%)	S_{BuOH} (%)	$Y_{2\text{-MF}}$ (%)	C (%)
Fe_{15}	573	32	90.8	4.6	1.6	3.0	0.0	29.1	2.1
Fe_{15}	550	40	94.0	2.2	1.0	2.0	0.8	37.6	4.1
Fe_{15}	523	6	100.0	0.0	0.0	0.0	0.0	6.0	1.4
$Pt_{1.7}$	573	100	0.0	0.5	0.0	99.3	0.2	0.0	0.1
$Pt_{1.7}$	550	100	2.7	22.4	5.1	69.8	0.0	2.7	1.0
$Pt_{1.7}$	523	100	0.0	55.4	5.8	38.8	0.0	0.0	1.8
$Fe_5Pt_{0.5}$	573	100	1.8	34.6	5.0	28.6	30.0	1.8	0.5
$Fe_5Pt_{0.5}$	550	100	1.2	19.6	4.3	38.4	36.5	1.2	0.5
$Fe_5Pt_{0.5}$	523	100	6.7	11.6	28	36.7	17.0	6.7	1.4
$Fe_7Pt_{0.07}$	573	84	51.9	38.3	0.0	9.8	0.0	43.8	1.0
$Fe_7Pt_{0.07}$	550	63	64.3	24.8	1.5	7.9	1.5	40.6	2.3
$Fe_7Pt_{0.07}$	523	13	41.6	40.8	0.0	17.5	0.1	5.2	2.3

[a] Selectivity to light and totally hydrogenated compounds. 2-MF: 2-methyl furan; F: Furan; 2-MTHF: 2-methyl tetrahydrofuran; BuOH: n-butanol.

Table 7: Percentages of carbonaceous deposits on each portion of the Fe_{15} (black) and $Fe_7Pt_{0.07}$ (red) catalyst bed when furfural, 2-MF or Furan is fed as reagent in presence of H_2, during 2 h. Reaction temperature 573 K.

	Reactant					
	Furfural		2-MF		Furan	
	Fe_{15}	$Fe_7Pt_{0.07}$	Fe_{15}	$Fe_7Pt_{0.07}$	Fe_{15}	$Fe_7Pt_{0.07}$
Inlet	4.2	1.9	0.2	0.2	0.2	0.1
Middle	4.3	1.6	0.2	0.1	0.5	0.2
Outlet	2.4	1.0	0.1	0.06	0.6	0.6

Table 8: Coke deposition on different catalysts. Reaction conditions: see Figure 6.

Catalyst	Fe/Pt	% C
$Pt_{1.7}$	0	0.4
$Fe_5Pt_{0.5}$	10	0.7
$Fe_7Pt_{0.07}$	100	1.2
Fe_{15}	∞	2.5

Legends to Figures

Figure 1: XRD patterns for the fresh catalyst reduced at 773 K. (I)Fe_{15}; (II) Fe_5; (III) $Fe_7Pt_{0.07}$; (IV) $Fe_5Pt_{0.5}$; and (V) $Pt_{1.7}$. References: α-Fe (○); γ-Fe_2O_3 or Fe_3O_4 magnetite (■)

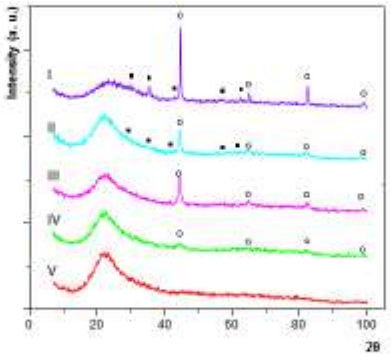

Figure 1

Figure 2: Temperature programmed reduction (TPR) profiles for the fresh catalysts. (I) Fe_{15}; (II) Fe_5; (III) $Fe_7Pt_{0.07}$; (IV) $Fe_5Pt_{0.5}$; and (V) $Pt_{1.7}$.

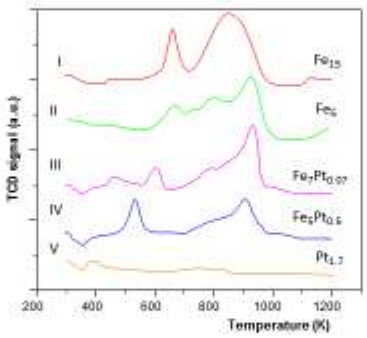

Figure 2

Figure 3: Mössbauer spectra of the reduced catalysts recorded at room temperature. (I) Fe_{15}; (II) Fe_5; (III) $Fe_7Pt_{0.07}$; and (IV) $Fe_5Pt_{0.5}$.

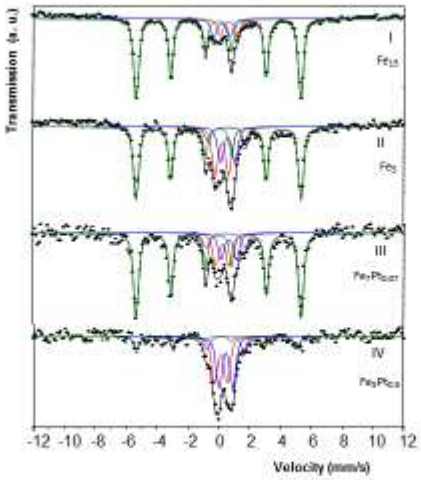

Figure 3

Figure 4: Activity and selectivities vs time on stream. T = 573 K. $W/F_{furfural}$ = 3 $g_{cat}.h.(g_{furfural})^{-1}$; W/F_{total} = 0.023 $g_{cat}.h.(g_{feed})^{-1}$; H_2/Furfural molar ratio = 245. (A) Fe_{15}; (B) $Pt_{1.7}$; (C) $Fe_5Pt_{0.5}$ and (D) $Fe_7Pt_{0.07}$. References: Conversion (Δ). Selectivity: light compounds (■); 2-methylfuran (●); furan (**x**); butanol (□); tetrahydrofuran (▲); 2-MTHF (♦); tetrahydrofurfuryl alcohol (♦); furfuryl alcohol (►).

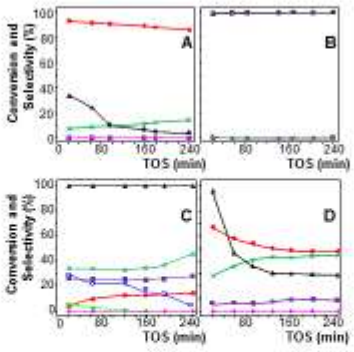

Figure 4

Figure 5: Temperature programmed Oxidation (TPO) profiles for (A) Fe_{15} and (B) $Fe_7Pt_{0.07}$ after reaction test $W/F_{furfural}$ = 3 $g_{cat}.h.(g_{furfural})^{-1}$; W/F_{total} = 0.023 $g_{cat}.h.(g_{feed})^{-1}$; H_2/Furfural molar ratio = 245, at (---) 523 K, (—) 550 K, and (···) 573 K.

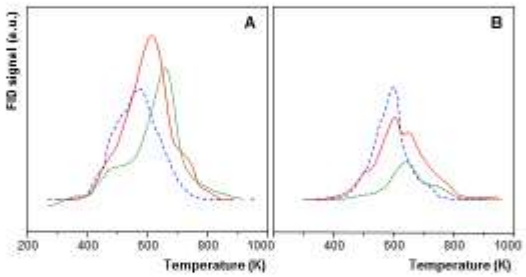

Figure 5

Figure 6: Temperature programmed oxidation (TPO) profiles for the catalyst tested at the same reaction conditions $W/F_{furfural}$ = 3 $g_{cat}.h.(g_{furfural})^{-1}$; W/F_{total} = 0.023 $g_{cat}.h.(g_{feed})^{-1}$; H_2/Furfural molar ratio = 245; T=573 K. (I) Fe_{15}; (II) $Fe_7Pt_{0.07}$; (III) $Fe_5Pt_{0.5}$; and (IV) $Pt_{1.7}$.

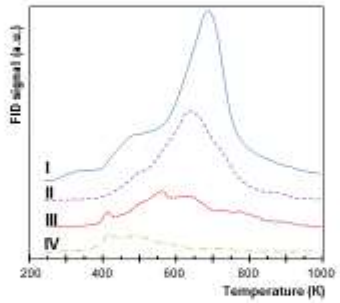

Figure 6

Figure 7: Conversion of furfural and selectivity to the different products vs time on stream of Fe_{15}.. T = 573 K, $W/F_{furfural}$ = 3 $g_{cat}.h.(g_{furfural})^{-1}$ and H_2/Furfural molar ratio: (A) 600, (B) 300 and (C) 100. References: Conversion (Δ). Selectivity: light compounds (■); 2-methylfuran (●); furan (**x**); butanol (□); tetrahydrofuran (▲); 2-MTHF (♦); tetrahydrofurfuryl alcohol (♦); furfuryl alcohol (►).

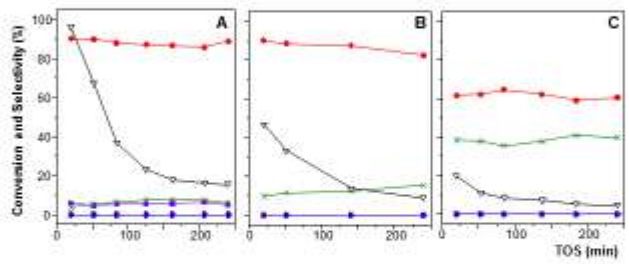

Figure 7

Figure 8: Catalyst Regeneration. The first regeneration treatment applied was with hydrogen at 773 K and the others with air at the reaction temperature. (A) Fe_{15}. Reaction temperature = 573 K; $W/F_{Furfural}$ = 3 $g_{cat}.h.(g_{furfural})^{-1}$; H_2/furfural molar ratio = 600. (B) $Fe_7Pt_{0.07}$. Reaction temperature = 550 K; W/F = 1.25 $g_{cat}.h.(g_{furfural})^{-1}$; H_2/furfural molar ratio = 168. Conversion (Δ). Selectivity: light compounds (■); 2-methylfuran (●); furan (**x**); butanol (□); tetrahydrofuran (▲); 2-MTHF (♦); tetrahydrofurfuryl alcohol (♦); furfuryl alcohol (►).

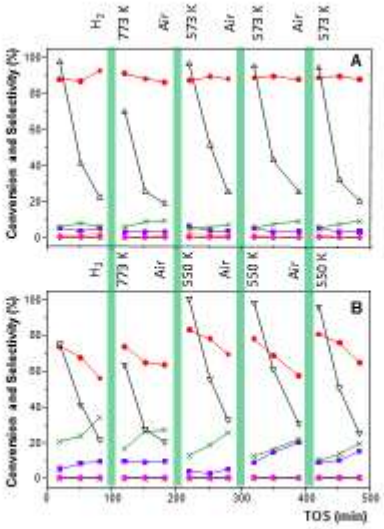

Figure 8

Scheme 1: Coke formation path.

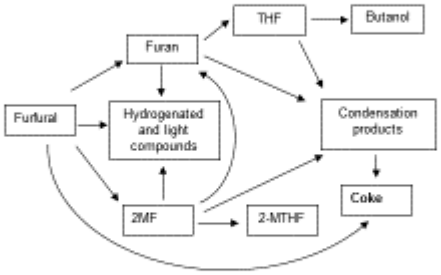

Scheme 1